Continental Shelf Research 137 (2017) 142–153

Contents lists available at ScienceDirect

Continental Shelf Research

journal homepage: www.elsevier.com/locate/csr

Observations of inner shelf cross-shore surface material transport adjacent to a coastal inlet in the northern Gulf of Mexico

Mathias K. Roth[a], Jamie MacMahan[a,*], Ad Reniers[b], Tamay M. Özgökmen[c], Kate Woodall[a], Brian Haus[c]

[a] Oceanography Department, Naval Postgraduate School, Monterey, CA 93943, United States
[b] Delft University of Technology, Delft, The Netherlands
[c] Rosentiel School of Marine and Atmospheric Science, University of Miami, Miami, FL 33149, United States

ARTICLE INFO

Keywords:
River Plume
Dispersion
Surface material transport
Nearshore
Coastal barriers
Surface drifters

ABSTRACT

Motivated by the Deepwater Horizon oil spill, the Surfzone and Coastal Oil Pathways Experiment obtained Acoustic Doppler Current Profiler (ADCP) Eulerian and GPS-drifter based Lagrangian "surface" (< 1 m) flow observations in the northern Gulf of Mexico to describe the influence of small-scale river plumes on surface material transport pathways in the nearshore. Lagrangian paths are qualitatively similar to surface pathlines derived from non-traditional, near-surface ADCP velocities, but both differ significantly from depth-averaged subsurface pathlines. Near-surface currents are linearly correlated with wind velocities (r =0.76 in the alongshore and r =0.85 in the cross-shore) at the 95% confidence level, and are 4–7 times larger than theoretical estimates of wind and wave-driven surface flow in an un-stratified water column. Differences in near-surface flow are attributed to the presence of a buoyant river plume forced by winds from passing extratropical storms. Plume boundary fronts induce a horizontal velocity gradient where drifters deployed outside of the plume in oceanic water routinely converge, slow, and are re-directed. When the plume flows west parallel to the beach, the seaward plume boundary front acts as a coastal barrier that prevents 100% of oceanic drifters from beaching within 27 km of the inlet. As a result, small-scale, wind-driven river plumes in the northern Gulf of Mexico act as coastal barriers that prevent offshore surface pollution from washing ashore west of river inlets.

1. Introduction

The Deepwater Horizon (DwH) oil spill (Aigner et al., 2010) demonstrated a need to further understand the physical processes that are important for the transport of oil at the surface of the nearshore region of the ocean (Dzwonkowski et al., 2014). The nearshore is the "last mile" for oil to transit to the beach and includes the surf zone, where waves break, and the inner shelf, defined by Lentz and Fewings (2012) as the region seaward of the surf zone, where the surface and bottom boundary layers overlap. As oil approached the Florida Panhandle in early June of 2010, nearshore surface oil forecasts available from the National Oceanic and Atmospheric Administration's (NOAA) Office of Response and Restoration relied upon satellite imagery and ocean circulation models that produced large "uncertainty boundaries" for where the oil would wash ashore (NOAA, 2010; Mariano et al., 2011). Oil location estimates were also inconsistent between forecasts (Mariano et al., 2011). Additionally, the spreading and mixing of surface material, defined as dispersion, is not predicted well by circulation models, particularly at the submesoscale (1–10 km) (Poje et al., 2014; Gildor et al., 2009). This challenge stems from anisotropic conditions near coastal boundaries where physical processes are non-homogeneous owing to dominant forcing mechanisms and response(s) that can change quickly with concomitant changes in water depth, inhibiting accurate parameterization of a bulk eddy diffusivity term (Swenson and Niller, 1996; LaCasce and Ohlmann, 2003; Haza et al., 2008; Romero et al., 2013). Field observations are necessary to increase knowledge of small-scale, anisotropic, nearshore transport processes and further develop oil forecasting capabilities.

Inner shelf circulation studies find that waves and winds are the principal forcing mechanisms for cross-shelf surface transport in the absence of stratification, as described in an inner shelf review article by Lentz and Fewings (2012) and briefly summarized here. When winds are absent, the Stokes drift velocities and wave-driven undertow balance each other at depth resulting in no net transport (Lentz et al., 2008). When the winds and waves are onshore, flow is onshore

* Corresponding author.Tel.:+1831 656 2379.
E-mail addresses: mkroth1@nps.edu (M.K. Roth), jhmacmah@nps.edu (J. MacMahan).

http://dx.doi.org/10.1016/j.csr.2016.12.017
Received 18 May 2016; Received in revised form 12 December 2016; Accepted 22 December 2016
Available online 28 December 2016

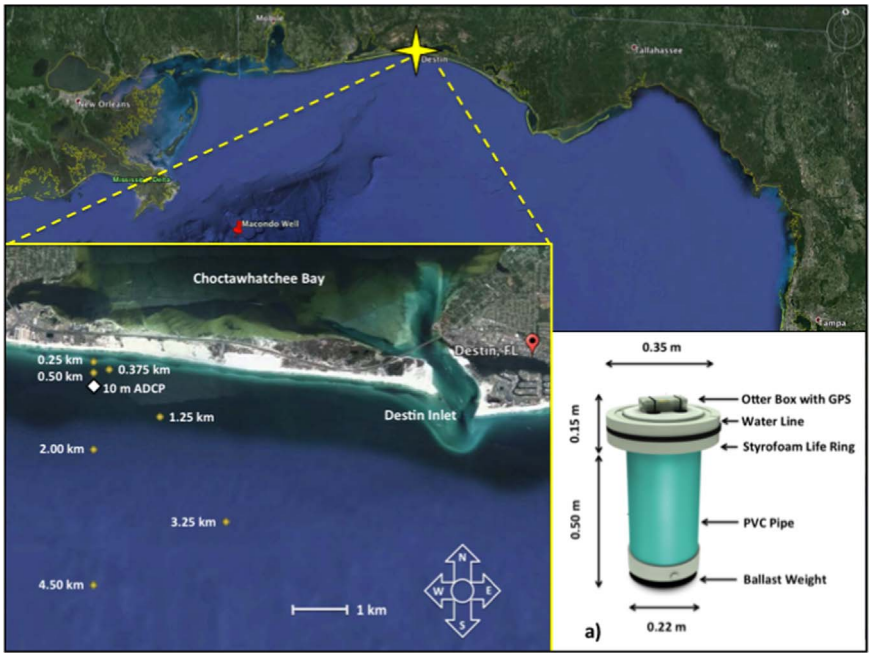

Fig. 1. Google Maps image of the northern Gulf of Mexico with SCOPE site indicated with a yellow star and the Macondo Well with a red marker to the southwest. Inner shelf drifter deployment locations are depicted by gold dots on zoom in of Destin Inlet and adjoining beach. 10 m ADCP is annotated with a white diamond and offset farther south for clarity. Inset a) SCOPE drifter with SPOT hand-held GPS affixed on top, inside an Otter Box.

near the surface and offshore at depth (Fewings et al., 2008; Hendrickson and MacMahan, 2009). Offshore winds and onshore waves result in strong offshore flow near the surface with decreasing offshore flow (Fewings et al., 2008) or onshore flow (Lentz and Fewings, 2012) at depth. As opposed to the mid- and outer continental shelves where cross-shore flow is driven by alongshore winds, cross-shore winds are more effective at driving cross-shore transport in the vertically well mixed inner shelf (Fewings, 2008; Lentz and Fewings, 2012; Dzwonkowski et al., 2011).

There have been fewer studies of cross-shore transport in stratified inner shelves, but for the stratified inner shelf in the northern Gulf of Mexico alongshore winds are more important for cross-shore transport than cross-shore winds (Dzwonkowski, 2011). Wind direction is also important for setting the orientation of river plumes as they emerge into the inner shelf of the northern Gulf of Mexico (Xia et al., 2011). Brackish, buoyant river plumes that emerge from coastal inlets are a source of stratification in the inner shelf and frequently add to coastal anisotropic conditions by propagating alongshore as a coastal current (Horner-Devine et al., 2015). When this occurs, the plume is typically a shallow surface feature (Chapman and Lentz, 1994) that deepens with downwelling winds (Haus et al., 2003) and extends stratification for tens of kilometers, or more, before mixing with the ambient oceanic water (Garvine, 1987; Yankovsky et al., 2000). Density fronts form as boundaries between the brackish riverine water and oceanic water (Garvine, 1987) and become submesoscale mechanisms for dispersion (Schroeder et al., 2012), where surface material converges and slows (Garvine, 1974; Garvine and Monk, 1974). Based on these studies it is expected that buoyant plumes within the inner shelf will alter the cross-shore transport of surface materials. However, to be useful in future oil spill prediction tools, the effect of the plume on cross-shore transport pathways needs to be further explored and quantified.

This study describes the Surfzone and Coastal Oil Pathways Experiment (SCOPE), performed in the inner shelf adjacent to Destin Inlet, Florida to explain the cross-shore surface transport of oil in the nearshore region during the Deepwater Horizon oil spill. As is common in inner shelf studies, water column velocity observations were collected using bottom-mounted Acoustic Doppler Current Profilers (ADCP). However, the common practice of removing observations from near-surface ADCP bins to avoid side lobe effects was not followed. This practice leads to a substantial loss of data in shallow waters (Dzwonkowski et al., 2014), and for the study of oil transport eliminates the critical layer of the water column where oil floated in the aftermath of the DwH spill (Kourafalou and Androulidakis, 2013). Instead, near-surface velocity observations below the wave trough level are retained while minimizing side lobe errors, as described in Section 2.3. To further overcome the deficiencies of the ADCP near-surface observations, GPS-drifters designed to float only in the top meter of the water column are employed to describe the Lagrangian surface behavior (Schmidt et al., 2003; MacMahan et al., 2009; Poulain, 1999), and are detailed in Section 2.2. Drifters have been successfully deployed to observe the variability of circulation patterns (Ohlmann and Niiler, 2005) and surface material dispersion in both the surf zone (Brown et al., 2009; MacMahan et al., 2010; Spydell et al., 2007) and inner shelf (Ohlmann et al., 2012). In addition to using drifters to observe circulation and dispersion, a unique comparison between drifter pathways and near-surface ADCP derived pathlines is employed to quantify the role of small-scale river plumes in cross-shore surface transport (Section 3). These findings highlight the formation of an important submesoscale, cross-shore transport barrier, it's frequency, persistence, and alongshore extent westward away from the inlet, which are then applied to the wind conditions that occurred during the DwH oil spill.

2. Materials and methods

2.1. Description of the field experiment

SCOPE was conducted in December 2013 at John Beasley Park (JBP) in Destin, FL along an open, nearly east-west oriented stretch of the NGoMex on a barrier island that was impacted by the Deepwater Horizon oil spill from the Macondo Well (Fig. 1). A cross-shore array of 4 RBR bottom Conductivity, Temperature, and Depth (CTD) sensors were deployed at 50 m, 100 m, 200 m, and 500 m from the beach in 1.5 m, 2.0 m, 3.0 m, and 10.0 m water depths. At the end of the array, collocated with the 10 m CTD, a bottom-mounted, upward-looking ADCP was deployed to collect pressure and along- (u) and cross-shore

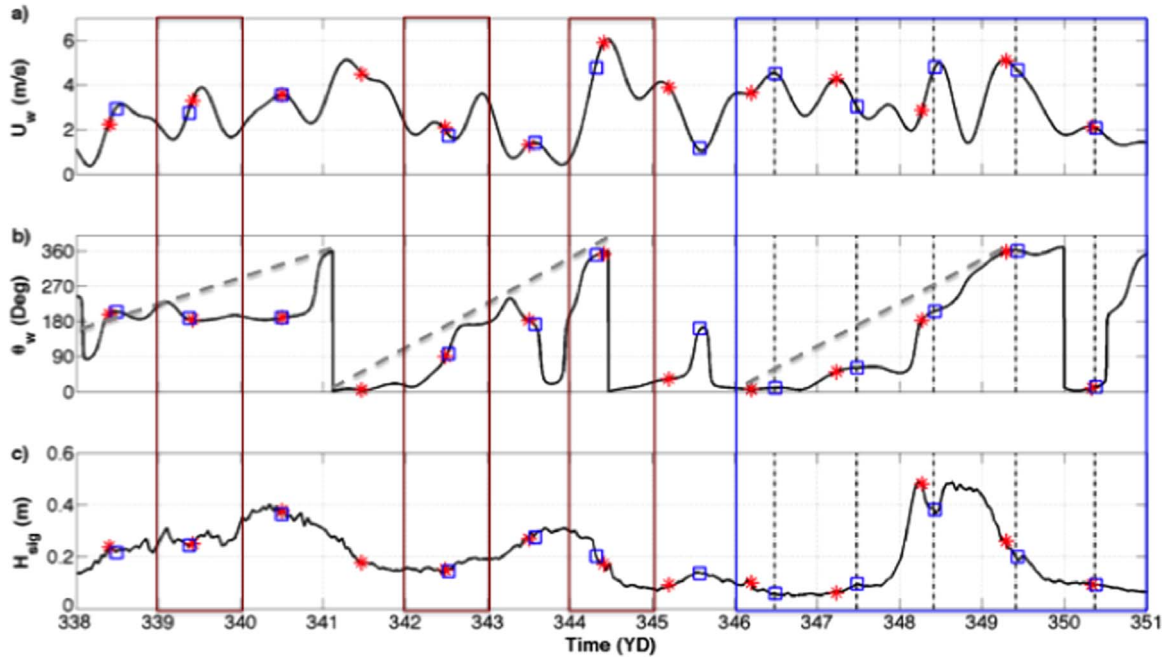

Fig. 2. a) SCOPE 6-min sampled wind speed and b) direction from the NOAA station Pensacola, FL (#8729840) low-pass filtered using a 12-h cut-off frequency. Gray dashed lines highlight the rotation of winds with the passage of winter storms. c) SCOPE hourly significant wave height. Brown boxes highlight drifter deployment in Destin Inlet on YD 339, 342, and 344. Blue box highlights the synoptic storm of interest and period of triplet drifter deployments. Black dashed lines indicate CTD cast times from 0.50 km drifter deployment station. Small blue squares represent the time that all drifters are in the water for each deployment. Red stars annotate low tide. No drifters were deployed on YD 341.

(v) velocity in 0.5 m bins continuously at 1 Hz for ~2 weeks (white diamond, Fig. 1).

During SCOPE, along- and cross-shore wind velocities were obtained using sonic anemometers mounted on a 10 m high mobile wind tower deployed in the backshore at JBP. Wind velocities were also obtained from NOAA Pensacola station located 75 km to the west of JBP (Fig. 2a,b). JBP and NOAA Pensacola wind velocities are correlated (r=0.72 and 0.92 for u and v) at the 95% confidence level. The wind velocities were low-pass filtered using a 12-h frequency cut-off. The Pensacola winds represent the mesoscale forcing, O(100 km). The JBP winds represent the local forcing effects associated with the nearby ADCP located directly offshore in 10 m water depth.

A series of low-pressure extratropical cyclones O(100 km) with moderate winds of magnitude O (5 m/s) that rotate 360° over 3–5 day periods passed from west to east during the experiment (gray lines, Fig. 2b). These synoptic storms are common during winter on the Florida Panhandle (Gutierrez de Velasco and Winant, 1996). Cross-shore winds (northerly and southerly) were most frequently observed at JBP (Fig. 3a). The fastest winds were most frequently from the north. In comparison, alongshore winds were less frequent but did, at times, blow with equal speed, O(5 m/s), from the east, northeast. Winds from the west were rarely observed.

Hourly significant wave heights were estimated by applying linear wave theory to convert the ADCP pressure observations to sea surface elevations (Guza and Thornton, 1980). The synoptic storm spanning YearDay (YD) 346–350 produced the largest waves observed during SCOPE, H_{sig} =~0.5 m (Fig. 2c). Throughout the experiment, the largest waves occurred when winds were from the south, ahead of frontal passage, which is consistent with the observations of Huh et al. (1984). When the winds were from any other direction, the presence of the coastline limited the available fetch, reducing wave heights (Fig. 2,b,c). The tides were primarily diurnal with 30 cm range. Low tide shifted ~0.75 h later each day.

During SCOPE, the Choctawhatchee River had a discharge of O(150 m^3/s), which is near the annual minimum. The river exited Destin Inlet into the inner shelf 7 km east of the experiment site with the ebb tide as a buoyant plume at the surface. Plumes are dynamically classified by the Kelvin Number,

$$K = \frac{\gamma L}{c/f}, \tag{1}$$

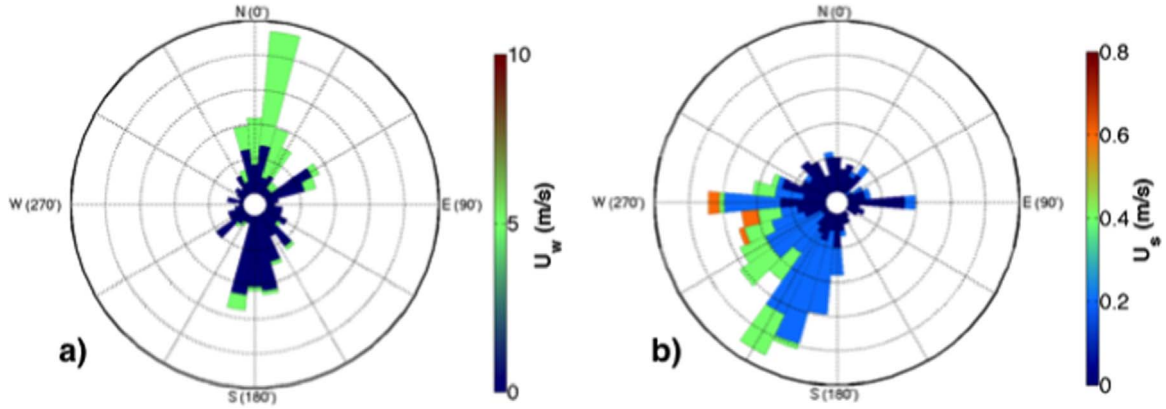

Fig. 3. Histograms of a) the hourly JBP wind (from) and b) the hourly surface current (to) during SCOPE.

in which the across-shore length scale of the discharge, γL, is defined as slenderness, γ, times the alongshore length of the discharge, L, and is compared to the baroclinic Rossby radius, c/f, defined by the internal wave phase speed, c, divided by the Coriolis parameter, f, (Garvine, 1995). Destin inlet has a depth of 7 m and width of 450 m (Valle-Levinson et al., 2015). Setting γL equal to the width of the inlet, assuming the initial depth of the plume is equal to the depth of the inlet, and using a representative observed density difference between the plume and ambient shelf water of 1.5 kg/m^3, Eq. (1) yields a Kelvin Number of 0.11. Because K «1, the Choctawhatchee Bay plume is classified as a small-scale plume (Garvine, 1995). The Choctawhatchee Bay plume is one of a series of small-scale wind-driven plumes in the NGoMex, which includes the Mobile Bay plume (Gelfenbaum and Stumpf, 1993) and Perdido Bay plume (Xia et al., 2011).

2.2. Description of SCOPE drifters & deployment schemes

More than 350 drifters were deployed from the beach, in the inlet, and in the inner shelf to observe surface (< 1 m) transport during SCOPE. Drifters deployed from the inner shelf on YD 346–350 targeted variability in the surface flow, expected from increased anisotropic conditions owing to the passage of a synoptic storm (Fig. 2 large blue box). They were deployed in the morning after the onset of ebb tide and after the plume had progressed out of the inlet and into the inner shelf (Fig. 2 blue squares and red stars). Each of the 5 deployments consisted of the release of 15 drifters from 7 stations in the inner shelf (Fig. 1 gold dots). At each of the 7 stations, a CTD was lowered through the water column coincident with drifter release to determine if the drifters were deployed in plume or oceanic water. Twelve drifters were launched in a triangular triplet configuration with O(1–10 m) initial separation distance at four cross-shore locations 0.25–4.50 km from the beach. The three remaining drifters were released at distances of 0.375 km, 1.25 km, and 3.25 km diagonally from the beach. The 75 drifters deployed over the 5-day period created a total of 525 original pairs of drifters for dispersion analysis with various initial separation distances. One of the locations of the drifter releases corresponded with the location of the ADCP for additional comparisons.

SPOT GPSs housed in small waterproof boxes were affixed to the top of the drifter (inset a, Fig. 1). The GPS transmitted their positions every 5 min for near real-time tracking and data archiving. The drifters were designed to be able to withstand and operate in the breaking waves of the surf zone while having a small surface expression to mitigate the effects of direct wind forcing, known as windage. Additionally, the drifters were made to be stackable and man-portable so that they could be deployed and re-deployed using small boats in multiple locations and in large quantities, which is important for Lagrangian statistics (LaCasce, 2008). The surface foam ring provided the appropriate buoyancy. A 5 lbs. weight was mounted on the bottom to create a lower center of mass, increase stability, and reduce surfing when drifters cross into the surf zone (Schmidt et al., 2003; MacMahan et al., 2009). Open holes at the top and bottom of the drifter allow water to free fill within the drifters and they submerge to just below the waterproof box. This creates a ~5 cm surface expression and minimal (< 7%) cross-sectional area that is exposed to wind while still enabling satellite communication.

During a qualitative experiment in Monterey Bay, SCOPE drifters and surf-zone drifters, designed by MacMahan et al. (2009), behaved similarly in the inner shelf. The surf-zone drifter is estimated to have a measurement error due to windage of ~0.01 m/s surface velocity per 1 m/s of wind velocity (MacMahan et al., 2010). SCOPE drifters have a smaller exposed cross-sectional area than surf-zone drifters because they do not have a 0.7 m antenna mast, but the same error due to windage is conservatively assumed.

2.3. Near surface velocity estimates from a bottom-mounted, upward-facing ADCP

Eulerian measurements of the surface flow can be obtained using a bottom-mounted, upward-facing ADCP, but the surface bin observations often have errors due to acoustic side lobe effects. A typical approach to remove these errors is to discard the upper two bins below the mean sea level (MSL). Depending on bin size, removal of two bins may leave only subsurface (> 1 m below MSL) velocity data available for analysis, which can be different than the surface (< 1 m below MSL) flow. To remove the effects of side lobe errors from the ADCP data, MSL and H_{sig} are computed every 15 min using linear wave theory. The 15-min quality control window represents stationarity for MSL and sea-swell waves. Velocity measurements above the MSL minus $H_{sig}/2$, referred to as the wave trough level, are discarded. Owing to the small tidal range and small waves during SCOPE, this technique removes 1 bin below the MSL (0–0.5 m below MSL). The two bins immediately below the wave trough level (0.5–1.5 m below MSL) are depth-averaged and used here to represent the near-surface flow. Note that this technique also removes Stokes drift from the observations. ADCP

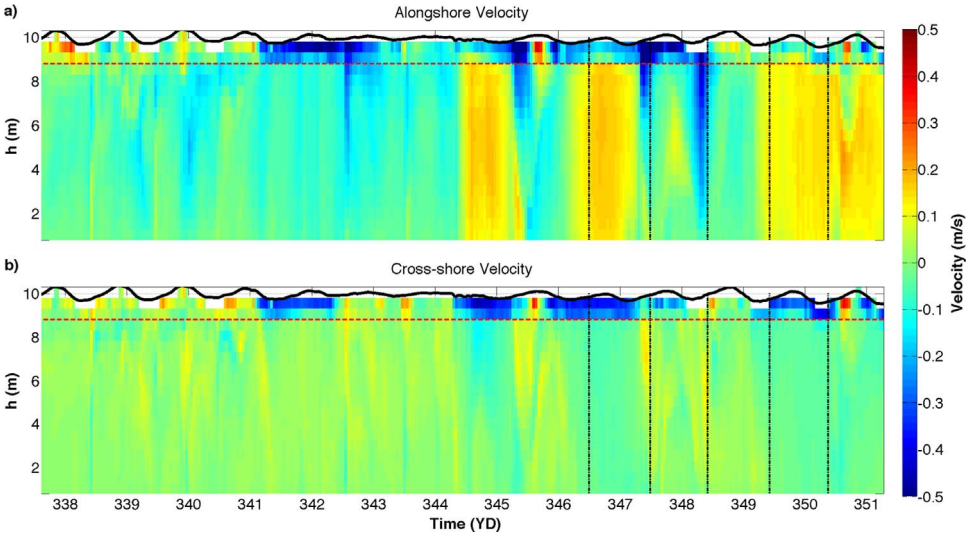

Fig. 4. a) ADCP alongshore, u, and b) cross-shore, v, hourly velocity profiles with depth for the 10 m ADCP. Positive velocities (red) are eastward and northward (onshore); negative velocities (blue) are westward and southward (offshore) in m/s. Black solid lines are the sea surface. Red dashed lines separate the surface layer from the subsurface layer. Vertical black dashed lines indicate CTD cast times from the 0.50 km drifter deployment station.

velocities are hourly-averaged by bin from 0.5 m above the bottom to the surface and presented in Fig. 4. Only observations below the wave trough level are kept. The red dashed lines at 8.5 m in Fig. 4 depict a clear delineation of surface versus subsurface flow structures, which often differ in magnitude and direction.

3. Results

Next, results for drifters deployed in the inlet and permitted to flow into the coastal ocean to track the plume orientation within the inner shelf (Section 3.1) are discussed. Then in Section 3.2, observed inner shelf currents are described by both drifters and ADCP during the passage of a synoptic storm to quantify the effect of the plume on surface flows. Salinity observations, drifter paths, and probability density functions of drifter movement follow to further elucidate the variability of surface transport in the inner shelf adjacent to the inlet (Section 3.3). Finally, an investigation of inner shelf anisotropic conditions is performed with the dispersion of drifters deployed into the surface layer.

3.1. River Plume variability in the inner shelf and coastal current formation

Drifters were deployed within the inlet during ebb tide to track the location of the plume as it emerges into the nearshore. Drifters were deployed on YD 339, 342, and 344 corresponding to days with light and variable, becoming southerly winds; weak winds with an easterly component; and moderate northerly winds (brown boxes Fig. 2). On YD 339 (blue lines Fig. 5), after the drifters exit the inlet, some move east and are pulled back into the inlet during the flood tide. Most proceed directly offshore before moving westward and onshore in an arcing pattern. These drifters trace a mid-field bulge and a far field coastal current down-coast, indicative of a prototypical plume (Horner-Devine et al., 2015). Drifters deployed during easterly winds on YD 342 do not extend as far offshore as the drifters on YD 339. These drifters do not show mid-field bulge development, and instead indicate that the outflow immediately turns west and forms a coastal current (red lines Fig. 5). This result is consistent with Fong and Geyer (2002), who find that an external mechanism, like wind, increases the freshwater input to the coastal current. When this occurs the coastal current deepens, widens, and increases in both speed and extent down the coast, as will be shown in Section 3.3. The enhanced coastal current is hereafter referred to as a coastal jet. Under moderate northerly winds on YD 344, the drifters emerge and continue directly offshore and neither the bulge, nor the coastal current forms (green lines Fig. 5).

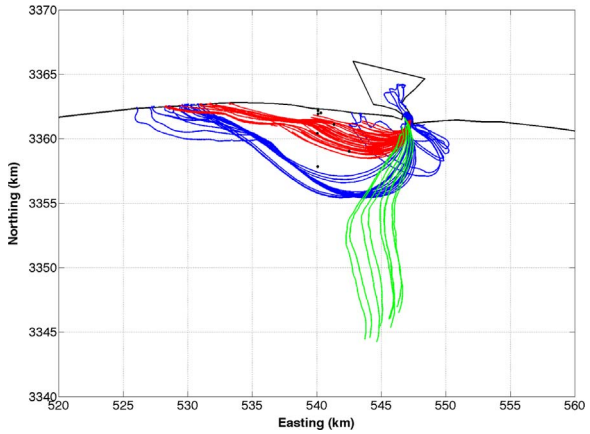

Fig. 5. Drifters deployed in the inlet on YD 339 (blue), YD 342 (red) and YD 344 (green) trace the plume into the inner shelf. Black circles near 540E are drifter deployment stations for YD 346–350 inner shelf drifter deployments.

3.2. Wind and Plume-driven surface flow patterns as observed with drifters and ADCP near-surface velocity estimates

The wind- and plume-driven surface flow in response to the passage of a synoptic storm is observed with both drifters and near-surface ADCP observations. To make comparisons between Lagrangian and Eulerian observations, pathlines (X, Y) are calculated by integrating the hourly (dt) subsurface and surface ADCP velocities (u and v) for the first 30 h (T) corresponding to drifter releases, where

$$X = \int_0^T u dt \tag{2}$$

and

$$Y = \int_0^T v dt. \tag{3}$$

The pathlines are compared to the trajectories of drifters deployed at the location of the ADCP (0.5 km offshore) on YD 346–350. The one exception is YD 348 when moderate southerly winds caused the drifters deployed at the 0.5 km station to beach quickly. On this day, drifter trajectories farther offshore (3.25 km) are used instead (Fig. 1).

Comparison of subsurface and surface pathlines during storm passage reveals that the surface current flows in different directions than the subsurface current (Fig. 6a,b). The subsurface current alternates exclusively northwest to southeast (Fig. 6a). In contrast, the surface current flows offshore to the south and west (Fig. 6b). Subsurface pathlines and drifter trajectories compare poorly in both direction and extent (Fig. 6a,b). Surface pathlines qualitatively match, but do not exactly replicate drifter trajectories due to inhomogeneities in the flow away from the ADCP (Fig. 6a,b). Windage and remaining side lobe errors may also contribute to discrepancies between surface pathlines and drifter trajectories. However, the agreement between surface pathlines and drifter trajectories, as compared to the poor agreement between the subsurface pathlines and drifter trajectories, highlights the importance of retaining ADCP observations in as many of the near-surface bins as possible. Near-surface bin retention is particularly important in the presence of a buoyant plume that provides stratification to the water column.

Surface pathlines and drifters trajectories both indicate that the surface flow responds to rotary winds associated with the synoptic storm. Surface currents and drifters flow south with northerly winds early on YD 346 and all day on YD 349 (Fig. 2b; Fig. 6b magenta and orange lines). Easterly winds on YD 347 drive a coastal jet (Fig. 2b; Fig. 6b red lines). The atmospheric front passes the experiment site on YD 348 and forces onshore surface flow early in the day followed by a rapid reversal to the south, offshore (Fig. 2b; Fig. 6b green lines). On YD 350 winds decrease to < 2 m/s and become variable (Fig. 2a,b). Light and variable winds lead to a small surface current that shifts between southwest and northeast until it flows consistently southwest, likely the result of the radial expansion of the plume bulge once it extends over the ADCP (Fig. 6b blue solid line).

The similarity between drifter trajectories and surface pathlines around the passage of a synoptic storm suggests that ADCP surface flow observations are useful for describing long term surface transport at this location. For all of SCOPE, near-surface ADCP velocities are significantly correlated at the 95% confidence level with the JBP wind speeds in the alongshore and cross-shore direction resulting in r-squared values, R^2, of 0.52 and 0.76. The associated linear slopes are 0.068 and 0.037, which represent the ratio of ADCP surface velocity to wind velocity. These ratios are higher than the theoretical ratio of 0.01 as estimated by the inner shelf vertical flow structure model of Lentz et al. (2008) using the wind and wave conditions observed during SCOPE (see Appendix A for more details). The high alongshore and cross-shore slope values are hypothesized to be an effect of the plume passing the ADCP as a coastal current, similar to the along- and cross-shelf flow ~10 km behind the leading edge of the coastal current

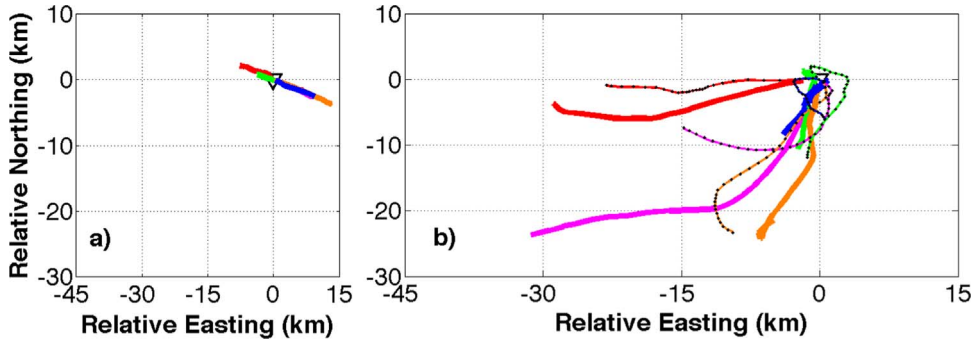

Fig. 6. a) 30-h pathlines of hourly depth-averaged ADCP subsurface (> 1 m) current compared with b) 30-h pathlines of ADCP surface current (< 1 m) (solid lines) and drifters (solid lines with black dots) for YD 346 (magenta), YD 347 (red), YD 348 (green), YD 349 (orange), and YD 350 (blue). Note the YD 348 drifter originates from the 3.25 km deployment station because the drifters at the 0.50 km station washed ashore within 7 h. The location of the ADCP is represented by a black triangle at 0E, 0N.

associated with Chesapeake Bay observed by Lentz et al. (2003). Hourly ADCP observations throughout SCOPE show that the surface layer flows predominantly to the southwest away from the beach, but frequently flows quickly along the coast (Fig. 3b). Fast westward flow is indicative of the presence of coastal currents and jets and supports the idea that the surface flows are both wind- and plume-driven.

3.3. SCOPE drifter fate and net transport direction

Throughout SCOPE, 355 drifters were deployed into the wind- and plume-driven surface layer. Salinity measurements from CTD casts during triplet deployments on YD 346–350 are used to categorize drifters deployed into the plume as plume drifters and drifters deployed outside the plume as oceanic drifters (Fig. 7a). CTD casts reveal that the freshest water is offshore and near the surface on YD 346. On YD 347, brackish water exists at all drifter deployment stations to a depth of 10 m, but is freshest at the coast. The three inshore stations remain fresh on YD 348. The water column is vertically mixed to an oceanic salinity across all four stations on YD 349 and YD 350, indicating that the plume has not reached the cross-shore array. The presence of coastal currents are inferred from wind and bottom salinity records to categorize drifters deployed within 300 m of the beach on YD 338, 343, 345, and 347 as plume drifters (Fig. 7b; Fig. 2a,b). Bottom salinity records show a cross-shore gradient of brackish water during predominantly southerly winds prior to YD 341. After YD 341, drops in salinity across the bottom CTDs appear to be related to the deepening and widening of the coastal current (Fig. 7b). All drifters deployed in the inlet are grouped as plume drifters.

Of the 216 plume drifters more than 90% beach within 27 km west of the inlet (Fig. 8a). The remaining ~10% move offshore to the south or southwest. Plume drifter paths reflect the net Eulerian surface flow alongshore and offshore observed by the ADCP (Fig. 3b). In contrast, oceanic drifters often travel far offshore in circuitous paths before returning towards the coast (Fig. 8b). When they do return to the coast these drifters often experience a deflection west within 27 km of the inlet (520 km E). 62 of the 139 oceanic drifters go directly to the beach during a period of sustained southerly winds from YD 338 through YD 340, at the beginning of the experiment (red lines, Fig. 8b).

Following a similar technique to that employed by Spydell et al. (2007) and Brown et al. (2009), 5-min position differences for 322 drifter records are used to construct probability density functions (PDF) of drifter displacements. Oceanic drifters (33) associated with 2

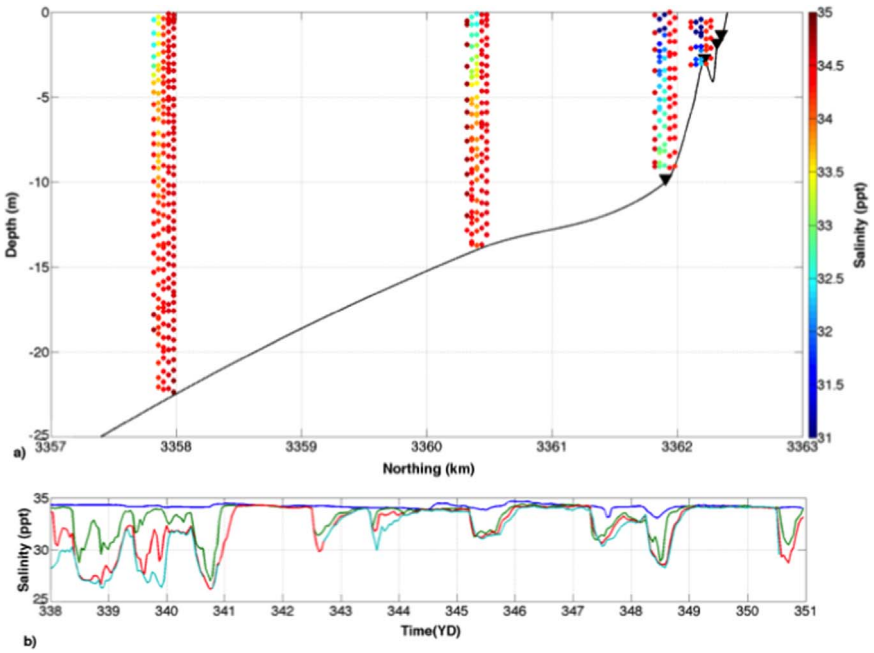

Fig. 7. a) Salinity observations with depth at the four cross-shore drifter deployment stations. CTD up-casts on YD 346 through YD 350 are depicted chronologically from left to right at each station. Black triangles near 3362N and shoreward represent the bottom CTD. b) Time series of salinity observations at the 10 m (blue), 3 m (green), 2 m (red), and 1.5 m (light blue) bottom CTD.

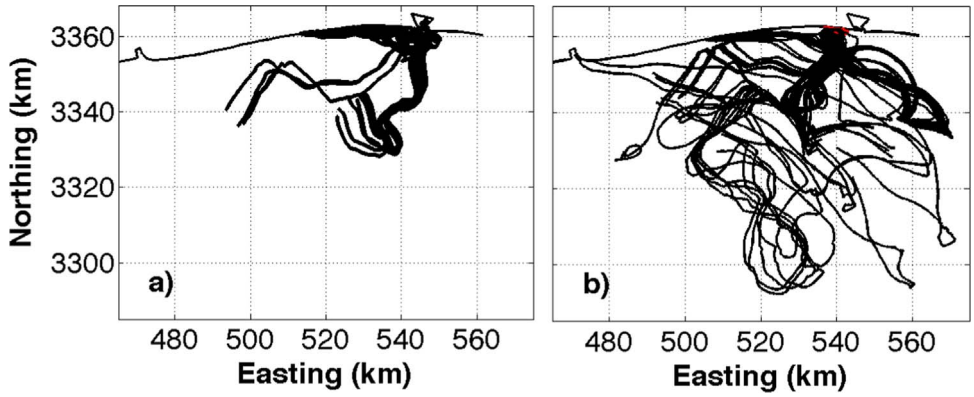

Fig. 8. Paths of drifters deployed a) into the plume and b) into oceanic water. Red lines in (b) represent oceanic drifters deployed close to the beach during sustained southerly winds that go directly onshore.

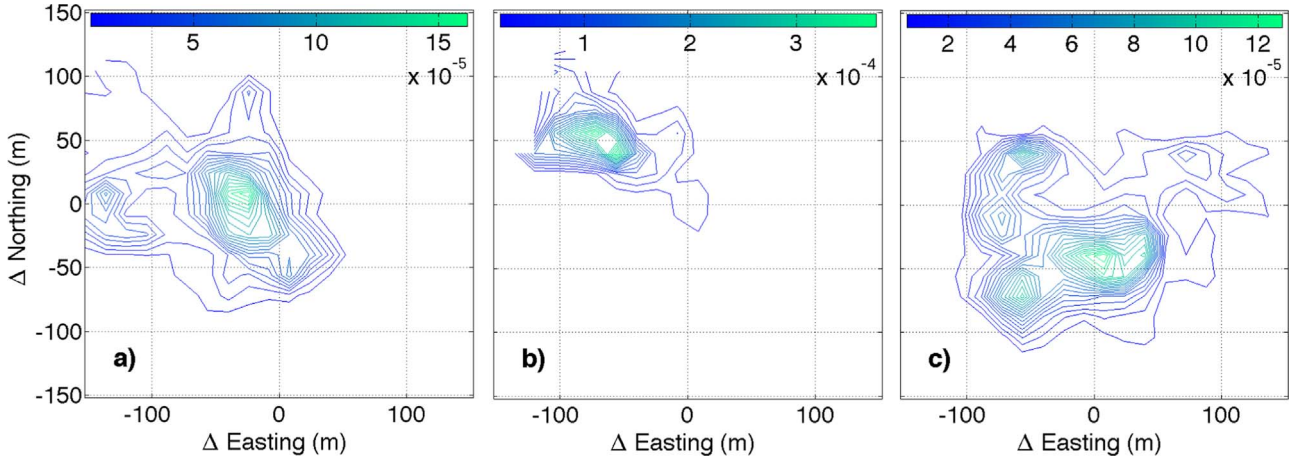

Fig. 9. Probability density functions for the most common displacement of a) plume drifters, b) oceanic drifters under sustained southerly winds, and c) oceanic drifters deployed during the approach and passage of a synoptic storm. Green contours are the most frequent displacement. Contours are normalized by both the number of drifters and the number of displacement bins.

extended inner shelf deployments form the majority of the long circuitous offshore paths in Fig. 8 and are left out of this analysis. A PDF is made for each of three categories of drifters, similar to those depicted in Fig. 8: plume, oceanic deployed during sustained southerly winds on YD 338 and YD 340, and oceanic deployed under rotary winds surrounding the synoptic storm, YD 346–350 (Fig. 9). The PDFs provide the most common five-minute magnitude and direction of movement of the drifters. The most common displacement for plume drifters is west along the coast with no preference in movement onshore or offshore (Fig. 9a). Oceanic drifters deployed near the beach during periods of sustained southerly winds also move west but are consistently forced north toward the beach (Fig. 9b). The oceanic drifters deployed around the storm transit primarily to the south or have a strong westward component to their cross-shore movement (Fig. 9c). The PDFs represent the net Lagrangian transport across the nearshore and complement the ADCP surface histogram (Fig. 3b) by showing that the plume forces surface material primarily west, parallel and south, away from the beach.

3.4. Drifter dispersion and anisotropy in the inner shelf

The continuous divergence and convergence of drifters over time is calculated statistically as the relative dispersion between pairs of drifters using the equation of variance (Spydell et al., 2007),

$$D_{ii}^2(t, s_0) = < [s_i(t) - s_{0i}]^2 > - < [s_i(t) - s_{0i}] >^2, \quad (4)$$

where s_{0i} is the initial pair separation distance at the time of deployment, $s_i(t)$ is the time-dependent pair separation distance, and angle brackets denote ensemble average. Eq. (4) is only valid for multiple pairs of drifters, and the calculation ceases when a drifter beaches or is recovered.

Inner shelf drifter deployments on YD 346–350 created 105 pairs daily for dispersion calculations. Plotting D^2 on a log-log scale allows determination of the power law between D^2 and t. On each day dispersion grows approximately as $D^2 \sim t^2$, indicative of local, ballistic dispersion caused by constant shear (LaCasce, 2008; Schroeder et al., 2012) (Fig. 10a). Though the observation of ballistic dispersion is

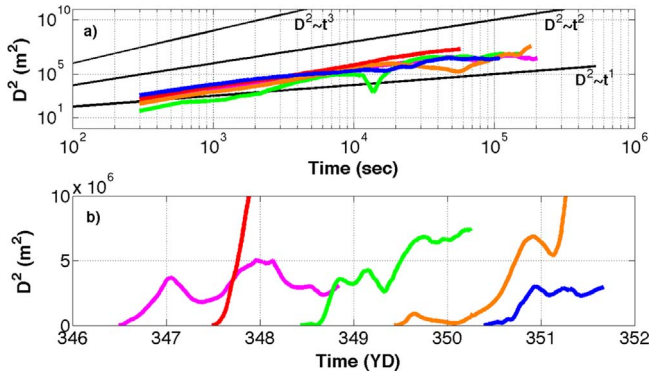

Fig. 10. a) Loglog plot of relative dispersion (D^2) for triplet deployments on YD 346 (magenta), YD 347 (red), YD 348 (green), YD 349 (orange), and YD 350 (blue) starting from the first position fix after release (300 s); b) linear plot of same D^2. Solid black lines are dispersion growth curves with time: Diffusive ($D^2 \sim t^1$), Ballistic ($D^2 \sim t^2$), and Richardson ($D^2 \sim t^3$).

consistent with the literature, there are large variations in growth between deployments and within each deployment, highlighting the anisotropic conditions present in the inner shelf. To attribute these variations to specific underlying physical processes, dispersion with respect to time is evaluated linearly to examine the finer details of D^2 growth (Fig. 10b). Of note, D^2 for YD 348 is calculated using only 4 drifters instead of 15 drifters because the 11 drifters deployed closest to shore beached quickly under the influence of southerly winds.

In the linear view, D^2 varies between the deployments, which represent different stages and wind directions of the synoptic storm. Initially (YD 346) the winds are northerly (Fig. 2a,b), and D^2 linearly increases before reaching a relative maximum (4×10^6 m^2) in 0.5 days (Fig. 10a magenta line). Dispersion begins to increase and decrease over the remainder of the deployment around an asymptotic mean of 4×10^6 m^2. As the storm approaches JBP on YD 347, D^2 increases exponentially (Fig. 10 red line), which is associated with the deployment of drifters into a coastal jet (described below). As the winds shift direction to southerly, D^2 increases linearly (Fig. 10 green line) before reaching a similar relative maximum (4×10^6 m^2) in ~0.25 days. Dispersion is relatively constant for half of a day before increasing again to another relative maximum (7×10^6 m^2) as winds shift to northerly and increase in speed on YD 349. There is minimal initial growth for the YD 349 deployment (Fig. 10 orange line) until YD350 when the winds become light and variable and dispersion increases to a maximum of 7×10^6 m^2 in 1 day. Dispersion on YD 350 also increases quickly under light and variable winds, but after 1 day oscillates about an asymptotic mean of 3×10^6 m^2 (Fig. 10b blue line), similar to YD 346.

When drifters from two deployments are in the water at the same time, D^2 can be similar, as is the case on the afternoon of YD 350 (Fig. 10b orange and blue lines). However, in general, periods of convergence and divergence that constitute D^2 are unique spatially by deployment (Fig. 10b.) This highlights the heterogeneity of the surface flow in the nearshore region, which in the NGoMex is related to mesoscale wind forcing and submesoscale plume-induced coastal currents and fronts.

3.4.1. Observations of a coastal jet and generation of coastal barriers

On YD 347, the wind direction shifts from northerly to northeasterly and the wind speed increases to 4 m/s at low tide (Fig. 2a,b). These easterly winds create a strong westward coastal jet that flows parallel to the beach away from the inlet, similar to the jet that existed on YD 342 when drifters were deployed in the inlet (Fig. 11; Fig. 5 red lines). The coastal jet is important for the mixing and transport in the nearshore region for two reasons: 1) it generates a horizontal velocity shear across the nearshore, and 2) it induces a coastal barrier that prevents surface material from moving onto the beach.

In addition to the 15 drifters deployed from the inner shelf stations, 17 drifters are deployed outside the surf zone in approximately 1.5 m water depth on YD 347. CTD casts observe a 0.7 kg/m^3 horizontal density gradient within the plume between the second and third cross-shore deployment stations with the least dense water near the beach (Fig. 11a blue and purple circles). CTD casts also indicate that the plume extends to at least 9 m depth at the 10 m ADCP (Fig. 7a). Drifters deployed within 1 km of the beach trace the jet as it moves 25 km westward, down-coast at speeds of ~0.5 m/s before beaching (Fig. 11a magenta arrows). The plume drifters deployed farther offshore also move westward, but at ~0.3 m/s or less before beaching 15 km away from the deployment stations (Fig. 11a black arrows). This coastal velocity shear is responsible for the exponential increase in D^2 (Fig. 10b red line). The YD 347 drifters all beach around the same time on YD 348, as the winds shift direction from easterly to southerly.

As the atmospheric front associated with the synoptic storm passes on YD 348, drifters deployed in oceanic water on YD 346 and YD 348 encounter the jet front between YD 348.5–348.7 and are barred from the beach (Fig. 2b; Fig. 11a,b). The YD 346 drifters, deployed during a moderate northerly wind, flow offshore initially (Fig. 11a). Easterly winds on YD 347 force the surface layer and YD 346 drifters to the west. Meanwhile, YD 347 drifters propagate down-coast within the newly developed coastal jet, as previously described. Soon after the start of YD 348, the wind shifts direction to southeasterly and the YD 346 drifters head toward the beach but hit the jet front, which acts as a coastal barrier, ~30 km west of the experiment site in the vicinity of 510E, 3358N and are redirected away from the coast (Fig. 11a).

An ADCP-derived surface pathline that originates at the time of the YD 348 drifter deployment indicates that the surface current near the ADCP continues west throughout YD 348 (Fig. 11b). Here, the coastal front acts as a barrier to prevent four oceanic drifters that are transiting to the north from washing ashore. Of the four drifters, the three western drifters, Triplet 190, converge along the front and then are forced west by it for ~5 h against the ambient surface current as winds shift clockwise out of the west, then northwest (Fig. 11b, Fig. 2b). During this period average speeds of Triplet 190 slow from ~0.24 m/s to less than 0.10 m/s. Conversely, Drifter 189 slows briefly when it meets the front, but bounces to the southeast and regains its previous speed of ~0.12 m/s. This difference in trajectory and speed between the four drifters during interaction with the coastal barrier increases dispersion from YD 348.6–348.8 (Fig. 10b green line). Following atmospheric frontal passage, all four drifters continue south with the surface current forced by northerly winds.

3.4.2. Observations of a weak coastal current and generation of coastal barriers

On YD 350, the plume expands from the inlet in all directions when the winds are light and variable, < 2 m/s (Fig. 2a,b). The boundary front associated with the plume bulge was visible ~0.50 km northeast of the 4.5 km deployment station due to convergence of foam and drifters, a darker color of water, and the congregation of birds (Fig. 12 arced solid blue line). Density differences are 1.5–2.0 kg/m^3, as measured by CTD casts on the west and east sides of the front near 541E, 3358N and 542E, 3361N (Fig. 12 red and blue circles). All drifters except one (542E, 3359N) are deployed in oceanic water. These drifters initially move southeast and then bounce off the bulge front and proceed to the west or northwest (Fig. 12 black lines and black arrows).

Closer to shore the front was visually observed to turn west and parallel the coast forming a coastal front (Fig. 12 solid blue line near 3362N). Drifters close to shore are barred from continuing to the beach by this coastal barrier and instead move along the front 0.50 km from the beach at speeds as high as 0.32 m/s until YD 350.7 when they turn to the south (Fig. 12 black arrows). In contrast, away from the coastal barrier, drifters deployed at the farthest offshore station continue north, not south, at YD 350.7 (Fig. 12 green segments with black arrows). By early YD 351 all drifters are moving south and begin to converge in the vicinity of 541E, 3355N. Multiple interactions between drifters and fronts throughout the deployment lead to circuitous drifter paths, shear and the observed dispersion (Fig. 10b blue line).

4. Discussion

Natural coastal barriers are aperiodically created depending on wind speed and direction. They are present when winds > 2 m/s have an easterly component and a coastal jet forms. Effective barriers also form when a weaker coastal current develops under light and variable winds (< 2 m/s). Wind speed and direction during ebb tide as the plume emerges are particularly important for barrier formation. During SCOPE, 8 of 13 days have winds that support barrier formation. Moderate winds with an easterly component during ebb tide are observed on YD 342, 345, 347 and 348. Light and variable winds during ebb tide are observed on YD 338, 339, 342, 343, and 350 (Fig. 2a,b).

The possibility of coastal barrier formation on eight days appears

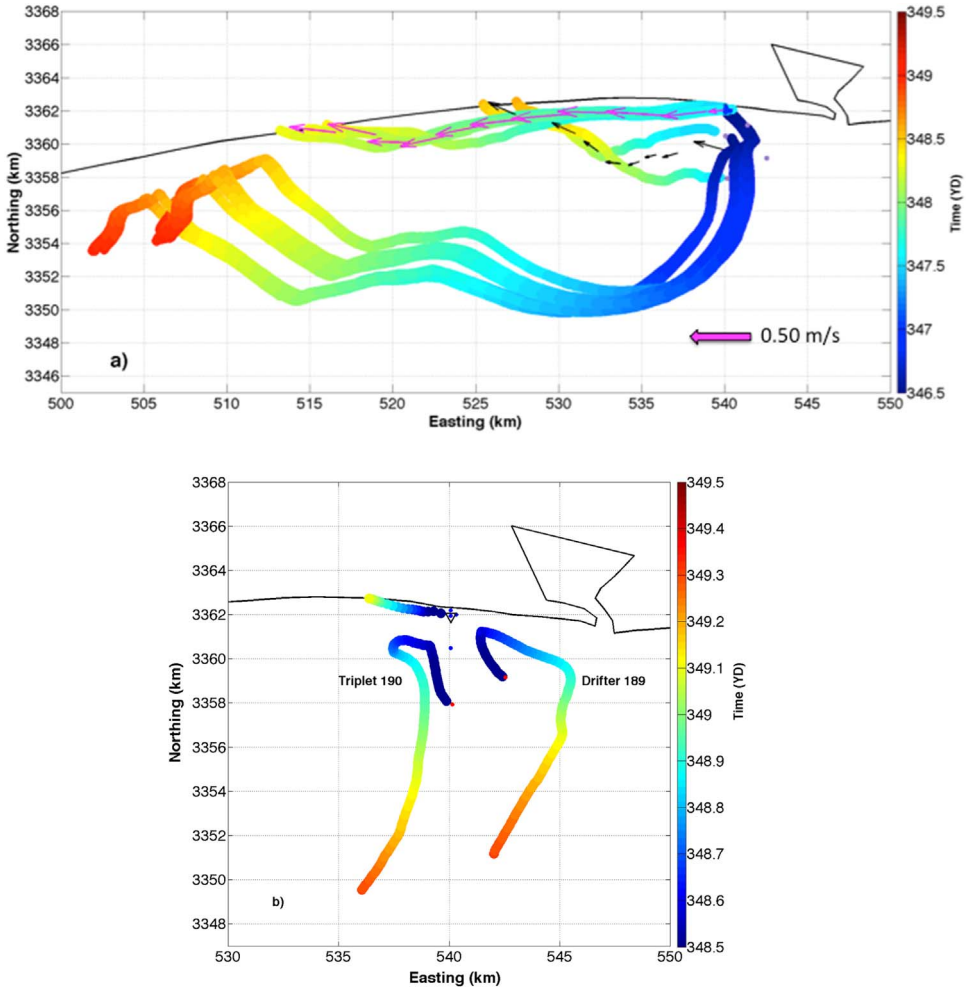

Fig. 11. a) Offshore, oceanic drifter trajectories scattered with time show that drifters deployed on YD 346 bounce off the YD 347 coastal jet west of 515E on ~YD 348.6. The jet is represented by drifter trajectories parallel to the beach and scattered with time. The jet is fastest near the coast (magenta arrows) inducing shear with slower currents offshore (black arrows). CTD casts during drifter deployment show that the plume is least dense at the coast (blue circles). Purple circles represent the increase in plume density offshore. b) Four oceanic drifters deployed on YD 348 encounter a coastal barrier and deflect offshore. The barrier is indicated by an ADCP surface pathline that shows a westward current at the coast during the time that the drifters change course away from the beach (~YD 348.6). Blue circles again indicate less dense plume water near the coast. Red circles indicate that the offshore drifters were deployed into dense oceanic water, as determined by CTD casts. Note (a) and (b) have different scales for Easting and Northing.

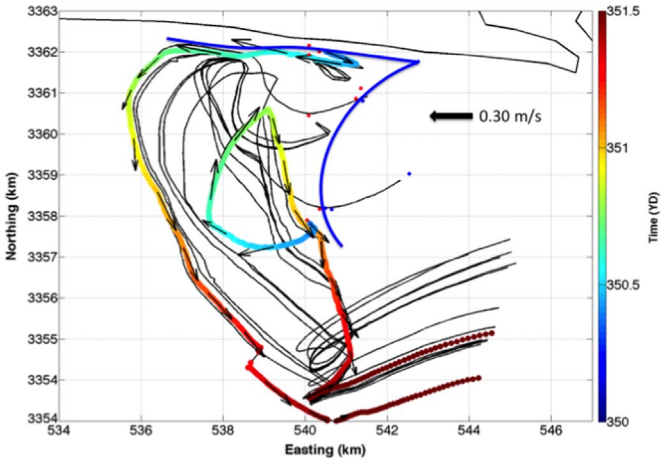

Fig. 12. Drifters bounce off the bulge front and then interact with the coastal front on YD 350 before proceeding to the southeast (black lines and black arrows). A drifter from the 0.25 km station traces the edge of coastal front along 3362N and is colored by time. A similarly colored trajectory shows that a drifter from the 4.5 km station moves in the opposite direction at YD 350.7, highlighting the importance of the coastal barrier to surface material transport under light and variable winds. Solid blue lines are the visually observed bulge and coastal fronts. Red and blue circles indicate oceanic or plume water during drifter deployment and corroborate the presence of the expanding bulge.

disproportionately high when considering the prevalence of moderate cross-shore winds compared to the frequency of moderate easterly or light and variable winds (Fig. 3a). However, rotary winds provide 2–3 opportunities for light and variable or easterly winds with the passage of each synoptic storm. Depending on the timing of these winds, formation of coastal barriers on 40–60% of days over a two-week period is reasonable, assuming 3 synoptic storms pass in two weeks. Sustainment of the barriers, however, appears to be tied to the persistence of the winds that formed the coastal barrier. This changes with each synoptic storm (gray dashed lines, Fig. 2b). The synoptic storm spanning YD 346–350 has the greatest period of moderate northeasterly winds of any of the three synoptic storms during SCOPE. These winds caused a coastal jet that persisted from YD 347 into YD 348, which is the longest observed.

Of the 75 drifters deployed from the inner shelf during passage of the synoptic storm (YD 346–350), the only drifters that made it to the beach were drifters deployed directly into the plume (26). Five more plume drifters and 44 oceanic drifters never washed ashore. Of the latter, 29 encountered the coastal barriers on YD 348 or YD 350 and were re-directed offshore (Fig. 11a,b; Fig. 12). The remaining 15 oceanic drifters did not beach because moderate northerly winds drove both the plume and ambient surface flow offshore. Coastal barriers prevent more plume and oceanic drifters from washing ashore than moderate northerly winds (34 to 26), even if the 11 oceanic drifters

that moved offshore initially with northerly winds on YD 346 are included in both groups (Fig. 11a). At synoptic storm time scales of ~5 days, coastal barriers are a significant physical mechanism that must be resolved to accurately determine the fate of surface material.

Results from the numerical modeling study by Xia et al. (2011) concerning the orientation of the wind-driven, small-scale Perdido Bay Estuary plume are consistent with the location of the Choctawhatchee Bay plume in the inner shelf under northerly and easterly winds. During no-wind conditions the Perdido Bay Estuary plume expands radially in all directions and is more expansive and less saline than plumes forced by strong winds from any particular direction (Xia et al., 2011). Radial expansion of the plume is consistent with bulge formation during SCOPE under light and variable wind conditions (Huguenard et al., 2016). The observed formation of coastal currents during these conditions are not reproduced by Xia et al. (2011), but are expected when the plume is unforced by winds (Fong and Geyer, 2002; Horner-Devine et al., 2015).

Modeled southerly winds have two effects on the plume: 1) they inhibit the plume from flowing out of the inlet; and 2) they cause a salt flux into the mouth of the bay that reduces the plume structure (Xia et al., 2011). A plume that successfully emerges during these conditions is expected to be closer in density to the ambient oceanic water than plumes forced by easterly or light and variable winds. The associated boundary fronts are likely to be weak and mix quickly with the ambient water, causing any barriers that form to be limited temporally and in spatial extent down the coast. No barriers, or weak barriers, are anticipated on days of sustained southerly winds, which matches observations of oceanic drifters that move quickly northwest to the beach during SCOPE (Fig. 8b red lines; Fig. 9b).

Winter coastal barriers can be predicted by tracking the formation and propagation of synoptic storms. This is particularly important in NGoMex where the winds associated with these storms may simultaneously force several plumes to protect or expose multiple stretches of the coastline to oceanic pollutants. The question of what the density difference needs to be between the inlet water and oceanic water to form an effective barrier at various distances from the inlet is left for future investigation. However, it is hypothesized that coastal barrier formation is less frequent and less effective during summer when predominantly southwest winds likely mix inlet waters to a near-oceanic salinity.

4.1. The wind regime hypothesis applied to the deepwater horizon oil spill

The SCOPE observations and findings are applied to winds that occurred during the DwH oil spill as a case study. From 20 April 2010 until 15 July 2010 oil spilled from the Macondo oil well 250 km southwest of the SCOPE site (Kourafalou and Androulidakis, 2013) (Fig. 1). Westerly winds < 5 m/s and the highest Mississippi River discharge during the active spill, 26,476 m^3/s on 28 May 2010, had pushed the resulting surface oil patch to ~88°W and 30°N, 25 km directly south of Mobile Bay and 73 km west of Pensacola by 01 June 2010 (YD 152) (Kourafalou and Androulidakis, 2013). This marked the greatest northeast extent of the surface patch to that point in the spill. Prior to YD 152, the farthest east that oil had been confirmed to have washed ashore was Petite Bois Island, MS, just west of the Mississippi-Alabama (MS-AL) border (YD 147), according to the NY Times online oil spill tracker (Aigner et al., 2010).

Winds shifted and became southerly at the end of May and increased to > 5 m/s from YD 154–157 near the Mississippi Delta, indicative of summer winds in NGoMex (Gutierrez de Velasco and Winant, 1996; Kourafalou and Androulidakis, 2013; Valle-Levinson et al., 2015). Pensacola winds also shifted direction and became southerly by YD 151 and increased to ~5 m/s on YD 154. Predominantly southerly winds persisted through YD 166 and the surface oil patch spread along the Florida Panhandle past Destin (Kourafalou and Androulidakis, 2013). As expected of beaches unprotected by coastal barriers, oil and/or tar balls started washing ashore (Aigner et al., 2010). Tar balls were confirmed to have arrived at Dauphin Island, AL on YD 153. On YD 155, oil and tar balls arrived along a 65 km stretch of the Florida Panhandle from Perdido Key to Navarre Beach. Oil was confirmed at Fort Walton Beach, FL, 10 km west of Destin Inlet on YD 156 (05 June), well within the extent of the coastal barrier had it existed.

5. Conclusion

A nearshore experiment (SCOPE) was conducted in an inner shelf within the northern Gulf of Mexico influenced by a river plume to determine how surface material, like oil, transits from deep water offshore to the beach. ADCP surface velocity observations, typically discarded from data analysis, are retained and indicate that wind and plume are the principal contributors to the speed and direction of the surface flow (< 1 m) 500 m offshore. Wind and plume-driven surface velocities are ~4–7 times greater than the theoretical value of the wind and wave-driven surface currents. Despite prevalent cross-shore winds, the surface flow is predominantly southwest away from the beach (Fig. 3). ADCP pathlines highlight the independence of the surface and subsurface flows (Fig. 6). Surface pathlines are useful for determining periods when the plume is oriented along the coast as a coastal current or jet (Fig. 11b).

The Choctawhatchee Bay plume, classified as a small-scale, wind-driven plume, adds heterogeneity to the nearshore by bringing cool, brackish water to the denser inner shelf water when it emerges from the inlet (Fig. 13). Plume boundary fronts are sources of shear that alter how drifters transit across the region and contribute to drifter dispersion O(5×10^6 m^2) (Fig. 10). Oil approaching the beach from offshore is also expected to converge and spread along plume boundary fronts (Fig. 13). Near the coast, the greatest dispersion ($> 1\times10^7$ m^2) occurred when fast coastal jets O(0.5 m/s) are generated by moderate winds (> 2 m/s) with an easterly component. Coastal jets are an extension of the plume westward, parallel to the coast. A similar but weaker coastal current develops during periods of light and variable winds (< 2 m/s). For both scenarios, drifters converge and change direction at the seaward coastal boundary front (Fig. 11; Fig. 12). These

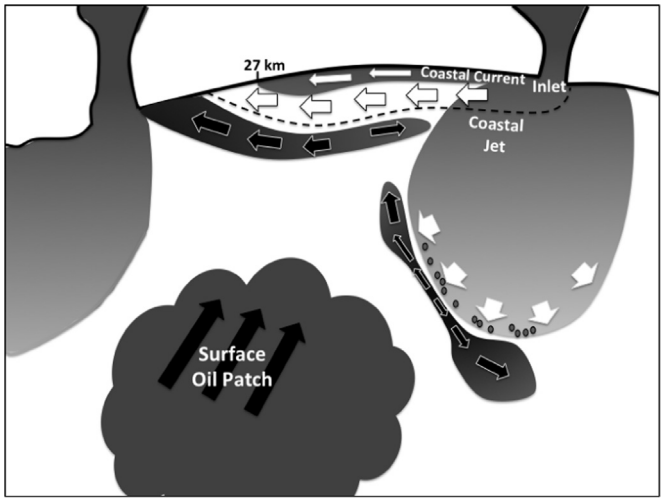

Fig. 13. A small-scale buoyant river plume expands into the inner shelf creating a mid-field bulge and thin far field coastal current under no wind conditions. A comparatively wide and fast coastal jet emerges without formation of the bulge during periods when winds exceed 2 m/s and have an easterly component (black dashed line). Offshore oil is pushed up against the boundary front associated with both the bulge and coastal current or jet. Oil spreads along each front and the coastal front becomes a coastal barrier. Oil only reaches the beach in locations where the coastal barrier is absent. White arrows are cool, brackish estuarine water; black arrows are oil. Small dark dots inside the plume bulge represent flotsam and other surface material that align along the front.

coastal barriers are 100% effective at barring drifters deployed outside the plume from beaching within 27 km west of Destin Inlet, and are expected to similarly prevent oil from washing ashore (Fig. 13).

The presence of the plume in the inner shelf enhances the anisotropic conditions found in the coastal ocean and further challenges ocean circulation models to resolve submesoscale features that are needed to determine the detailed movement and fate of offshore oceanic pollutants. However, predictions of when and where oil will transport to the beach can be improved by forecasting the winds that cause coastal barrier formation. Natural coastal barriers are present during ~50% of the synoptic storm cycle and are as effective at preventing surface material from washing ashore as moderate northerly winds that force the surface layer offshore. In both cases no drifters beach. These findings are particularly important in the northern Gulf of Mexico where a series of river inlets separated by distances < 100 km may be forced simultaneously by mesoscale winds to create barriers along long stretches of the coast during the passage of synoptic storms (Fig. 13). During periods of moderate southerly winds when coastal barriers are absent or ineffective, oceanic pollution moves unimpeded to the beach, as it did in June 2010 following the Deepwater Horizon oil spill. In addition to improving prediction capabilities, wind- and plume-driven natural coastal barriers should be considered as part of the strategy to combat future oil spills and have implications for ecological, economic, and public health policies.

Acknowledgements

The data for this paper are available online at www.data.gulfresearchinitiative.org as MacMahan, Jamie, CARTHE: SCOPE experiment CTD casts, Santa Rosa Island, Florida, December 2013; MacMahan, Jamie, CARTHE: SCOPE experiment cross-shore array measurements, Santa Rosa Island, Florida, December 2013; and MacMahan, Jamie, CARTHE: SCOPE experiment surface drifters, Santa Rosa Island, Florida, December 2013. The data are distributed by: Gulf of Mexico Research Initiative Information and Data Cooperative (GRIIDC), Harte Research Institute, Texas A&M University-Corpus Christi. This work was supported by the Gulf of Mexico Research Initiative (GoMRI). Thanks to E. B. Thornton for helpful suggestions. Thank you to Keith Wyckoff, Kyle Baden, Jenna Brown, Conor Smith and all those who participated in the launch and recovery of drifters during SCOPE. Appreciation is extended to Ping Zhu for the use of wind data at JBP and to Steven Lentz for the use of his undertow model. The Office of Naval Research, to whom we are grateful, purchased much of the equipment used in SCOPE through a Defense University Research Instrumentation Program. Additional thanks are offered to Mike Cook for assistance with data analysis, and to Shawn Gallaher and Matt Gough for discussions on the topic.

Appendix A

The theoretical value of the wind and wave-driven surface current is estimated with the Lentz et al. (2008) inner shelf model using observational ranges from SCOPE. The wind velocities obtained at a height of 9.6 m from the NOAA station Pensacola (#8729840) were converted to wind stress,

$$\tau = \rho_a C_D W^2, \tag{A1}$$

where ρ_a is the air density (1.22 kg/m^3), C_D is the drag coefficient (1.2×10^{-3}) and W is wind speed (0–6 m/s) corrected to an altitude of 10 m (Large and Pond, 1981; Pond and Pickard, 1983). The range of significant wave heights is computed from the ADCP deployed in 10 m water depth (Fig. 2c). A wave period of 3 s is used, representative of local wind-generated waves with short fetch observed during the experiment; the Coriolis parameter at JBP, 7.36×10^{-5} s^{-1}; and bottom roughness of $z_o = 10^{-3}$ m, consistent with Lentz et al. (2008) are also input to the model. The alongshore pressure gradient is assumed to be small and set equal to 0 m/s^2. The model-provided cubic eddy viscosity profile was selected following Fewings et al. (2008), who found that it provides realistic velocity profiles under cross-shore winds (Lentz, 1995; Lentz et al., 2008). Model results indicate that the wind and wave-driven surface current in the top 1 m of the water column is on average 1% of the observed wind speed (Fig. A1). The cross-shelf surface velocity shear profile during northerly winter winds at JBP is representative of enhanced flow at the surface caused by wind and undertow acting in the same direction, as described by Fewings et al. (2008).

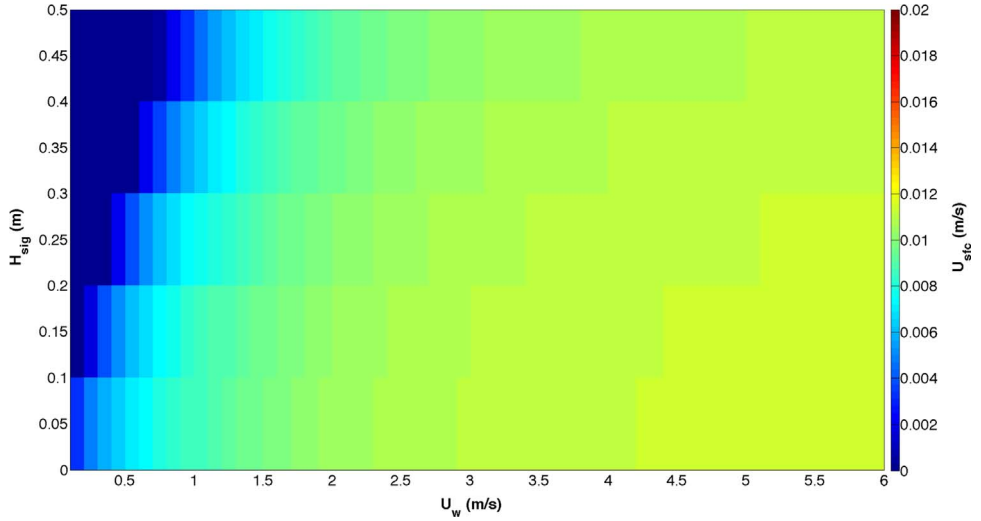

Fig. A1. The average 1-m surface current as a function of wind speed (U_w) and significant wave height (H_{sig}) calculated with the Lentz et al. (2008) wind and wave-driven inner shelf model.

References

Aigner, E., Burgess, J., Carter, S., Nurse, J., Park, H., Schoenfeld, A., Tse, A., 2010. Tracking the Oil Spill in the Gulf. NY Times Online.

Brown, J., MacMahan, J., Reniers, A., Thornton, E., 2009. Surf zone diffusivity on a rip-channeled beach. J. Geophys. Res. 114, C11015. http://dx.doi.org/10.1029/2008JC005158.

Chapman, D.C., Lentz, S.J., 1994. Trapping of a Coastal Density Front by the Bottom Boundary Layer. J. Phys. Oceanogr. 24, 1464–1479. http://dx.doi.org/10.1175/1520-0485(1994)024 < 1464:TOACDF > 2.0.CO;2.

Dzwonkowski, B., Park, K., Jiang, L., 2011. Subtidal across-shelf velocity structure and surface transport effectiveness on the Alabama shelf of the northeastern Gulf of Mexico. J. Geophys. Res. 116, C10012. http://dx.doi.org/10.1029/2011JC007188.

Dzwonkowski, B., Park, K., Lee, J., Webb, B.M., Valle-Levinson, A., 2014. Spatial variability of flow over a river-influenced inner shelf in coastal Alabama during spring. Cont. Shelf Res. 74, 25–34. http://dx.doi.org/10.1016/j.csr.2013.12.005.

Fewings, M., Lentz, S.J., Fredericks, J., 2008. Observations of cross-shelf flow driven by cross-shelf winds on the inner continental shelf. J. Phys. Oceanogr. 38, 2358–2378. http://dx.doi.org/10.1175/2008JPO3990.1.

Fong, D.A., Geyer, W.R., 2002. The alongshore transport of freshwater in a surface-trapped river plume. J. Phys. Oceanogr. 32, 957–972. http://dx.doi.org/10.1175/1520-0485(2002)032 < 0957:TATOFI > 2.0.CO;2.

Garvine, R.W., 1974. Dynamics of small-scale oceanic fronts. J. Phys. Oceanogr. 4, 557–569. http://dx.doi.org/10.1175/1520-0485(1974)004 < 0557:DOSSOF > 2.0.CO;2.

Garvine, R.W., 1987. Estuary plumes and fronts in shelf waters: a layer model. J. Phys. Oceanogr. 17, 1877–1896. http://dx.doi.org/10.1175/1520-0485(1987)017 < 1877:EPAFIS > 2.0.CO;2.

Garvine, R.W., 1995. A dynamical system for classifying buoyant coastal discharges. Cont. Shelf Res. 15, 1585–1596. http://dx.doi.org/10.1016/0278-4343(94)00065-U.

Garvine, R.W., Monk, J.D., 1974. Frontal structure of a River Plume. J. Geophys. Res. 79, 2251–2259. http://dx.doi.org/10.1029/JC079i015p02251.

Gelfenbaum, G., Stumpf, R.P., 1993. Observations of currents and density structure across a buoyant plume front. Estuaries 16, 40–52. http://dx.doi.org/10.2307/1352762.

Gildor, H., Fredj, E., Steinbuck, J., Monismith, S., 2009. Evidence for submesoscale barriers to horizontal mixing in the ocean from current measurements and aerial photographs. J. Phys. Oceanogr. 39, 1975–1983. http://dx.doi.org/10.1175/2009JPO4116.1.

Gutiérrez de Velasco, G., Winant, C.D., 1996. Seasonal patterns of wind stress and wind stress curl over the Gulf of Mexico. J. Geophys. Res. 101, 18127–18140. http://dx.doi.org/10.1029/96JC01442.

Guza, R.T., Thornton, E.B., 1980. Local and shoaled comparisons of sea surface elevations, pressures, and velocities. J. Geophys. Res. 85, 1524–1530. http://dx.doi.org/10.1029/JC085iC03p01524.

Haus, B.K., Graber, H.C., Shay, L.K., Cook, T.M., 2003. Alongshelf variability of a coastal buoyancy current during the relaxation of downwelling favorable winds. J. Coast. Res. 19 (2), 409–420.

Haza, A.C., Poje, A.C., Özgökmen, T.M., Martin, P., 2008. Relative dispersion from a high-resolution coastal model of the Adriatic Sea. Ocean Model. 22, 48–65. http://dx.doi.org/10.1016/j.ocemod.2008.01.006.

Hendrickson, J., MacMahan, J., 2009. Diurnal sea breeze effects on inner-shelf cross-shore exchange. Cont. Shelf Res. 29, 2195–2206. http://dx.doi.org/10.1016/j.csr.2009.08.011.

Horner-Devine, A.R., Hetland, R.D., MacDonald, D.G., 2015. Mixing and transport in coastal river plumes. Annu. Rev. Fluid Mech. 47, 569–594. http://dx.doi.org/10.1146/annurev-fluid-010313-141408.

Huguenard, K.D., Bogucki, D.J., Ortiz-Suslow, D.G., Laxague, N.J.M., MacMahan, J.H., Özgökmen, T.M., Haus, B.K., Reniers, A.J.H.M., Hargrove, J., Soloviev, A.V., Graber, H., 2016. On the nature of the frontal zone of the Choctawhatchee Bay plume in the Gulf of Mexico. J. Geophys. Res. Oceans 121, 1322–1345. http://dx.doi.org/10.1002/2015JC010988.

Huh, O.K., Rouse, L.J., Jr., Walker, N.D., 1984. Cold air outbreaks Over the northwest Florida continental shelf: heat flux processes and hydrographic changes. J. Geophys. Res. 89, 717–726. http://dx.doi.org/10.1029/JC089iC01p00717.

Kourafalou, V.H., Androulidakis, Y.S., 2013. Influence of Mississippi River induced circulation on the Deepwater Horizon oil spill transport. J. Geophys. Res. Oceans 118, 3823–3842. http://dx.doi.org/10.1002/jgrc.20272.

LaCasce, J.H., 2008. Statistics from Lagrangian observations. Prog. Oceanogr. 77, 1–29. http://dx.doi.org/10.1016/j.pocean.2008.02.002.

LaCasce, J.H., Ohlmann, C., 2003. Relative dispersion at the surface of the Gulf of Mexico. J. Mar. Res. 61, 285–312. http://dx.doi.org/10.1357/002224003322201205.

Large, W.G., Pond, S., 1981. Open ocean momentum flux measurements in moderate to strong winds. J. Phys. Oceanogr. 11, 324–336. http://dx.doi.org/10.1175/1520-0485(1981)011 < 0324:OOMFMI > 2.0.CO;2.

Lentz, S.J., 1995. Sensitivity of the inner-shelf circulation to the form of the eddy viscosity profile. J. Phys. Oceanogr. 25, 19–28. http://dx.doi.org/10.1175/1520-0485(1995)025 < 0019:SOTISC > 2.0.CO;2.

Lentz, S.J., Fewings, M.R., 2012. The wind- and wave-driven inner-shelf circulation. Annual Rev. Mar. Sci. 4, 317–343. http://dx.doi.org/10.1146/annurev-marine-120709-142745.

Lentz, S.J., Elgar, S., Guza, R.T., 2003. Observations of the Flow Field near the Nose of a Buoyant Coastal Current. J. Phys. Oceanogr. 33, 933–943. http://dx.doi.org/10.1175/1520-0485(2003)33 < 933:OOTFFN > 2.0.CO;2.

Lentz, S.J., Fewings, M., Howd, P., Fredericks, J., Hathaway, K., 2008. Observations and a model of undertow over the inner continental shelf. J. Phys. Oceanogr. 38, 2341–2357. http://dx.doi.org/10.1175/2008JPO3986.1.

MacMahan, J., Brown, J., Thornton, E., 2009. Low-cost handheld global positioning system for measuring surf-zone currents. J. Coast. Res. 253, 744–754. http://dx.doi.org/10.2112/08-1000.1.

MacMahan, J., Brown, J., Brown, J., Thornton, E., Reniers, A.J.H.M., Stanton, T., Henriquez, M., Gallagher, E., Morrison, J., Austin, M., Scott, T., Senechal, N., 2010. Mean Lagrangian flow behavior on an open coast rip-channeled beach: a new perspective. Mar. Geol. 268, 1–15. http://dx.doi.org/10.1016/j.margeo.2009.09.011.

Mariano, A.J., Kourafalou, V.H., Srinivasan, A., Kang, H., Halliwell, G.R., Ryan, E.H., Roffer, M., 2011. On the modeling of the 2010 Gulf of Mexico oil spill. Dyn. Atmospheres Oceans 52, 322–340. http://dx.doi.org/10.1016/j.dynatmoce.2011.06.001.

National Oceanic and Atmospheric Administration, Office of Response and Restoration, 2010. Field Guide to NOAA's Oil Trajectory Maps. ⟨www.response.restoration.noaa.gov⟩.

Ohlmann, J.C., Niiler, P.P., 2005. Circulation over the continental shelf in the northern Gulf of Mexico. Prog. Oceanogr. 64, 45–81. http://dx.doi.org/10.1016/j.pocean.2005.02.001.

Ohlmann, J.C., Lacasce, J.H., Washburn, L., Mariano, A.J., Emery, B., 2012. Relative dispersion observations and trajectory modeling in the Santa Barbara Channel. J. Geophys. Res. 117, C05040. http://dx.doi.org/10.1029/2011JC007810.

Poje, A.C., Özgökmen, T.M., Lipphardt, B.L., Haus, B.K., Ryan, E.H., Haza, A.C., Jacobs, G.A., Reniers, A.J.H.M., Olascoaga, M.J., Novelli, G., Griffa, A., Beron-Vera, F.J., Chen, S.S., Coelho, E., Hogan, P.J., Kirwan, A.D., Jr., Huntley, H.S., Mariano, A.J., 2014. Submesoscale dispersion in the vicinity of the Deepwater horizon spill. Proc. Natl. Acad. Sci. 111, 12693–12698. http://dx.doi.org/10.1073/pnas.1402452111.

Pond, S., Pickard, G.L., 1983. Introductory Dynamical Oceanography 2nd ed. Butterworth-Heinemann, Woburn, M. A..

Poulain, P.-M., 1999. Drifter observations of surface circulation in the Adriatic Sea between December 1994 and March 1996. J. Mar. Syst. 20, 231–253. http://dx.doi.org/10.1016/S0924-7963(98)00084-0.

Romero, L., Uchiyama, Y., Ohlmann, J.C., McWilliams, J.C., Siegel, D.A., 2013. Simulations of nearshore particle-pair dispersion in Southern California. J. Phys. Oceanogr. 43, 1862–1879. http://dx.doi.org/10.1175/JPO-D-13-011.1.

Schmidt, W.E., Woodward, B.T., Millikan, K.S., Guza, R.T., Raubenheimer, B., Elgar, S., 2003. A GPS-tracked surf zone drifter. J. Atmos. Ocean. Technol. 20, 1069–1075.

Schroeder, K., Chiggiato, J., Haza, A.C., Griffa, A., Özgökmen, T.M., Zanasca, P., Molcard, A., Borghini, M., Poulain, P.M., Gerin, R., Zambianchi, E., Falco, P., Trees, C., 2012. Targeted Lagrangian sampling of submesoscale dispersion at a coastal frontal zone. Geophys. Res. Lett. 39, L11608. http://dx.doi.org/10.1029/2012GL051879.

Spydell, M.S., Feddersen, F., Guza, R.T., Schmidt, W.E., 2007. Observing surf-zone dispersion with drifters. J. Phys. Oceanogr. 37, 2920–2939. http://dx.doi.org/10.1175/2007JPO3580.1.

Swenson, M.S., Niller, P., 1996. Statistical analysis of the surface circulation of the California Current. J. Geophys. Res. 101, 22631–22645. http://dx.doi.org/10.1029/96JC02008.

Valle-Levinson, Huguenard, K., Ross, L., Branyon, J., MacMahan, J., Reniers, A.J.H.M., 2015. Tidal and nontidal exchange at a subtropical inlet: destin inlet, Northwest Florida. Estuar. Coast. Shelf Sci. 155, 137–147. http://dx.doi.org/10.1016/j.ecss.2015.01.020.

Xia, M., Xie, L., Pietrafesa, L.J., Whitney, M.M., 2011. The ideal response of a Gulf of Mexico estuary plume to wind forcing: its connection with salt flux and a Lagrangian view. J. Geophys. Res. 116, C08035. http://dx.doi.org/10.1029/2010JC006689.

Yankovsky, A.E., Garvine, R.W., Münchow, A., 2000. Mesoscale currents on the inner New Jersey shelf driven by the interaction of buoyancy and wind forcing. J. Phys. Oceanogr. 30, 2214–2230. http://dx.doi.org/10.1175/1520-0485(2000)030 < 2214:MCOTIN > 2.0.CO;2.